Molecular dynamics of silicon indentation

J. S. Kallman, W. G. Hoover, C. G. Hoover, A. J. De Groot, S. M. Lee, and F. Wooten
Department of Applied Science Davis-Livermore, Lawrence Livermore National Laboratory, Livermore, California 94550
(Received 30 September 1992)

We use nonequilibrium molecular dynamics to simulate the elastic-plastic deformation of silicon under tetrahedral nanometer-sized indentors. The results are described in terms of a rate-dependent and temperature-dependent phenomenological yield strength. We follow the structural change during indentation with a computer technique that allows us to model the dynamic simulation of diffraction patterns.

Low-cost parallel computers are revolutionizing the scope of computational physics and its impact on materials science. These machines are ideally suited to large-scale simulations of high-strain-rate elastic-plastic flows involving millions of degrees of freedom.[1,2] We have used pair potentials typical of simple materials like rare gases, as well as embedded-atom collective potentials used to describe metals.[2] Here we extend our investigations to silicon, which exhibits several solid phases stabilized by strong covalent bonds. For simplicity we use the Stillinger-Weber model for the pair and many-body silicon potentials.[3]

The present paper describes our simulation of the nanometer-sized indentation process and our development of a diagnostic diffraction tool for following structural changes during simulation. We expect that further development along these same lines will help determine the potential machinability on the micrometer and nanometer scales of nominally brittle materials in order to guide design processes. Sufficiently deep cuts *always* cause cracks. With micrometer-scale indentation, crystalline silicon develops surface cracks. But because crack energy varies as the $\frac{2}{3}$ power of specimen size, simple dimensional reasoning (the surface-to-volume energy ratio) suggests that, at a *sufficiently small* scale, indentation (or cutting) *must* be crack free.[4] Computer simulation can make this qualitative argument quantitative.

Laboratory indentation experiments are simulated as is shown in Fig. 1. Silicon, just beneath the indentor, has been claimed[5,6] to undergo *two* different pressure-induced solid-solid phase transformations: to the high-pressure (above about 100 kbars) β-Sn structure and to the thermodynamically unstable but well-characterized *amorphous phase.*

To investigate the simulated microstructure of silicon, before, during, and after indentation, we simulate the diffraction process. Computational diffraction photo-

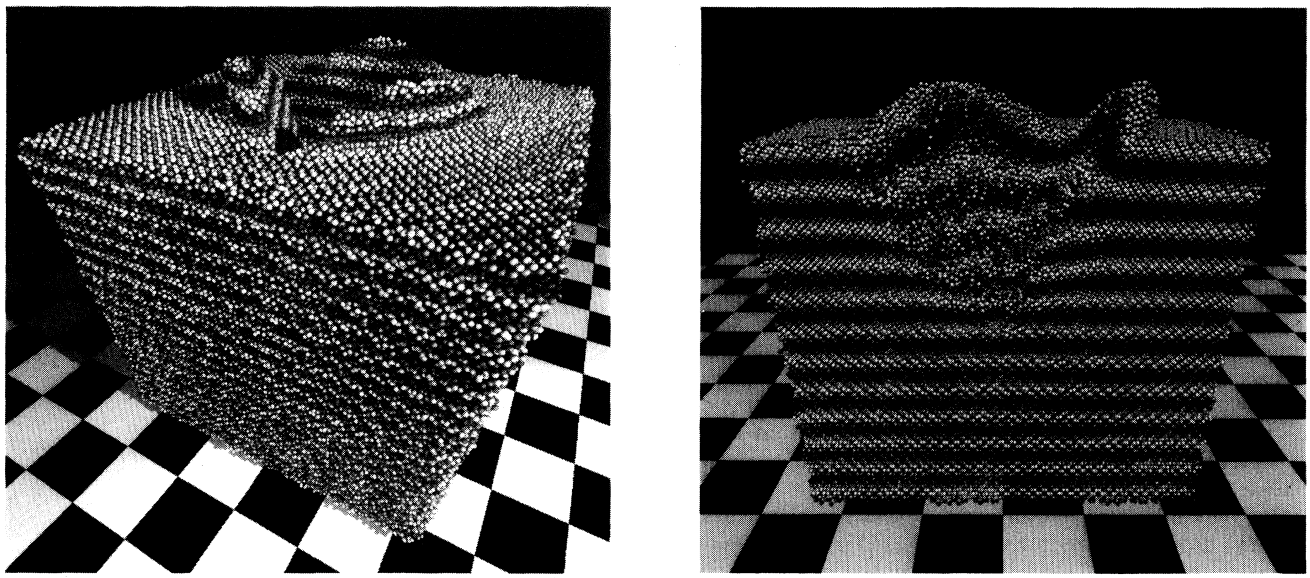

FIG. 1. The simulated indentation of crystalline Stillinger-Weber silicon. The left-hand view shows 373 248 silicon atoms, indented at a speed of 0.5 (about one sixth the speed of sound) and at a temperature $kT=0.03$, about half the melting temperature. The right-hand cutaway view of the same simulation reveals the plastic deformation in the vicinity of the indentation. The shading of the (left/right) figure is based on the (final/initial) vertical coordinates of the atoms.

graphs are produced by exposing a selected portion of the computational workpiece to a monochromatic coherent wave. The resulting *computational* patterns closely approximate electron or x-ray *laboratory* diffraction patterns.

We present here atomistic indentation results for both amorphous and single-crystal silicon as well as a description of diffraction patterns which characterize the structure. Simultaneously we extract thermodynamic information from the simulation, the work done and the heat generated during the indentation process.

To simulate *isothermal* deformation, we incorporate Nosé-Hoover constraint forces[1,7] F_c in all our finite-temperature simulations. These constraint forces $F_{\text{constraint}} \equiv -\zeta p \equiv -\zeta m\dot{r}$ satisfy integral feedback relations based on the time-integrated kinetic energy $K \equiv \Sigma(m/2)\dot{r}^2$ and the characteristic response time τ. In finite-difference form the Nosé-Hoover equations of motion become[7]

$$m(r_+ - 2r_0 + r_-)/dt^2 = F_0 - m\zeta_0(r_+ - r_-)/(2\,dt) , \quad (1)$$

$$(\zeta_+ - \zeta_-)/(2\,dt) = [\Delta K_0/\langle K\rangle]/\tau^2 ,$$
$$K_0 = \Sigma m(r_+ - r_-)^2/(8\,dt^2) , \quad (2)$$

where the subscripts $\{-,0,+\}$ indicate the time sequence $\{t-dt, t, t+dt\}$. In three space dimensions, the mean value of the kinetic energy $\langle K\rangle$ is $(\frac{3}{2})NkT$. The response time τ is on the order of atomic-vibration times. The forces $F(r_0)$ are based on Stillinger and Weber's pair and three-body force model.[3] We chose not to investigate the alternative Tersoff potential because the corresponding force law contains unphysical singularities.[8]

The Stillinger-Weber model includes both two- and three-body contributions:

$$\Phi_2 \equiv \Sigma 7[0.6r^{-4} - 1]\exp[(r-1.8)^{-1}] \quad \text{for } r < 1.8,$$
$$\Phi_3 \equiv \Sigma 21 \exp[1.2(r_{ji}-1.8)^{-1} + 1.2(r_{ik}-1.8)^{-1}][\cos\theta + \tfrac{1}{3}]^2 \quad \text{for } r_{ji} < 1.8 \text{ and } r_{ik} < 1.8 .$$

To create a correspondence between our computer simulation and "real" silicon we use the energy, mass, and length units adopted by Stillinger and Weber, 50 kcal/mol, 4.65×10^{-23} gm, and 0.21 nm, respectively. In these units the energies of fusion and boiling are 0.22 and 1.4 for an atom of real silicon; the mass of an atom is unity, and the range of the Stillinger-Weber potential function is 1.8.

In our *computational* hardness tests, we use both "smooth" continuum and "rough" atomistic indentors, shaped as regular tetrahedra in both cases. Thus the border of an indentation pit is an equilateral triangle of the type shown in Fig. 1. To simulate the indentation of amorphous silicon, we start out with a 32 768-atom-annealed solid based on a $2\times2\times2$ array of 4096-atom amorphous unit cells constructed by Wooten and Weaire.[9] Similar structures have been generated before.[10]

In the case of our *smooth* indentor, each atom in the workpiece interacts with the *closest* point of an idealized perfect tetrahedron using the short-ranged repulsive Lennard-Jones potential, $\phi(r) = 1 + r^{-12} - 2r^{-6}$, for $r < 1$. In the case of our *atomistic* indentor, each atom in the workpiece interacts, according to this same truncated Lennard-Jones potential, with all the atoms in an fcc indentor which lie within a distance $r < 1$. In this case, the indentor atoms occupy portions of [111] planes, forming a regular tetrahedron. The increase in the work of deformation, resulting from the use of a rough indentor, can be about 35%. Thus the isothermal work of deformation is only somewhat sensitive to the indentor boundary condition.

Laboratory diffraction patterns use x rays, neutrons, or electrons to map out a Fourier transform of a spatial array of atoms. A crystal provides a pattern of Bragg-diffraction spots. A liquid, or an amorphous solid, provides instead a pattern of diffuse concentric rings around the straight-ahead direction of the diffraction beam. Because our computer-generated videotapes of the indentation process show no signs of fluidity with the isothermal simulations well below the melting point, we believe that the liquid phase of Stillinger-Weber silicon is not formed in these simulations. Figure 2 is a computational diffraction pattern corresponding to the Wooten-Weaire

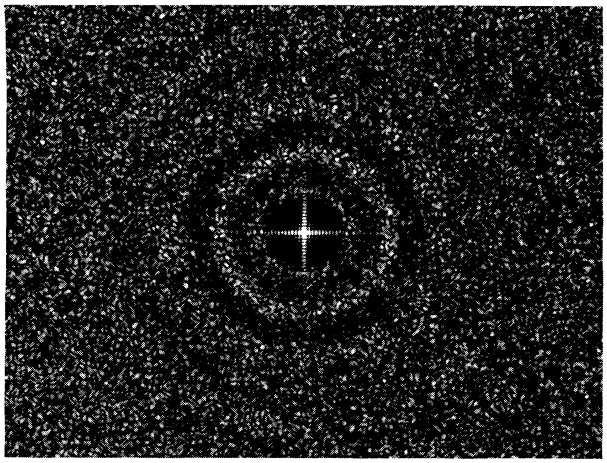

FIG. 2. The computational diffraction pattern for the Wooten-Weaire amorphous silicon structure used in our indentation simulations.

4096-atom amorphous silicon sample which we have used in our indentation work. We found that about 100 atoms are required to characterize a crystal spot pattern or an amorphous ring pattern. By sampling regions localized in space and time, it is possible to follow the structural progress of phase transformations. We have used this tool to study deforming solids during the indentation process.

To generate a diffraction pattern, we first consider a "beam" propagating in the x direction, so that a phase $\phi_i \equiv \exp[ikx_i]$ is associated with an atom i at a distance x_i from the beam source. Next, we consider a "film," an imaginary computational plane divided into a grid (typically 1024×1024) of pixels. In this picture, each atom broadcasts a spherical wave (with wave number k) corresponding to a scattering of the initial plane wave (also with wave number k and with phase $\exp[ikx_i]$). The diffraction pattern at the film is then computed by summing the phases $\exp[ikx_i]\exp[ikr_{ij}]$ at each pixel j from all atoms i of interest in the sample. The distance between scattering atom i and exposed pixel j is r_{ij}. Such a computational process is ideally suited to parallel computation. Each processor is assigned to carry out the simulated diffraction process for a particular set of pixels. At completion, the magnitude of the summed phases from all the atoms is plotted at the film position. In Fig. 3, we display 36 of a set of $6\times6\times6=216$ diffraction patterns [001 direction] obtained from an indented crystal. In this case, with $kT=0.06$, there is clear evidence for an amorphous structure indicated by the diffuse rings in patterns generated from atoms near the indentor. At melting, kT is about 0.06_6.

In addition to these Fourier representations of solid structure, we have also considered an angle-averaged "pair distribution function" $G(r)$. This function is the number density of atoms at r divided by r. For a structureless amorphous material with a constant number density N/V, $G(r)$ would be $4\pi rN/V$. The three silicon structures considered here differ qualitatively in the peak positions of the corresponding $G(r)$. We found it particularly useful to construct "bar-code" plots of $G(r)$, representing that function in shades of grey. In Fig. 4 we compare the bar-code plots for both the amorphous and the diamond structures. Such data indicate, through the disappearance of the third peak in the diamond-structure pattern, the appearance of amorphous material near the indentor.

To analyze the simulation data, we have taken into account three approximately separate contributions to the work of indentation, $W=W_{\text{strain}}+W_{\text{surface}}+W_{\text{plastic}}$.

(1) In linear elasticity, the strain energy is quadratic in the displacement: $W_{\text{strain}}\propto V^{2/3}$, where V is the indentation volume, $3^{1/2}H^3/8$ for a tetrahedral indentation of height H.

(2) The surface energy is likewise quadratic in the displacement: $W_{\text{surface}}\propto V^{2/3}$, where V is again the indentation volume.

(3) The plastic deformation energy is proportional to the volume of indentation: $W_{\text{plastic}}\propto V$.

Accordingly we have fitted the dynamic work of deformation, as a function of the height of the indentation cavity H (proportional to time), to a two-term function of volume, $\alpha H^2+\beta H^3$, identifying the latter term with the plastic work of indentation W_{plastic} (see Fig. 5). The fit is

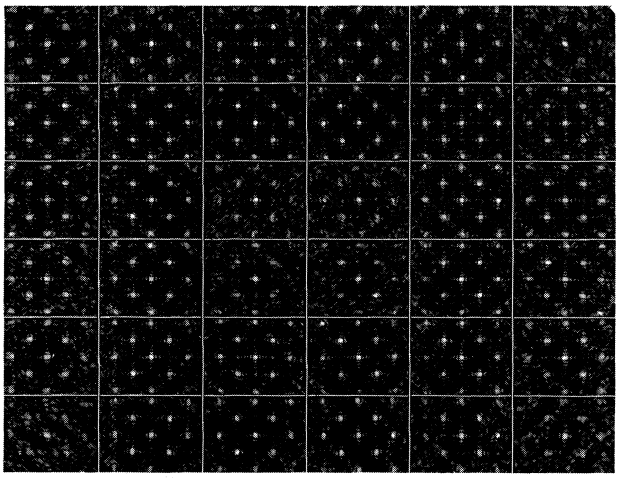

FIG. 3. 36 diffraction patterns from cubes just above the midplane of a 32 768-atom-indented silicon crystal with $kT=0.06$, just below the melting point. The speed of the smooth indentor was 0.1.

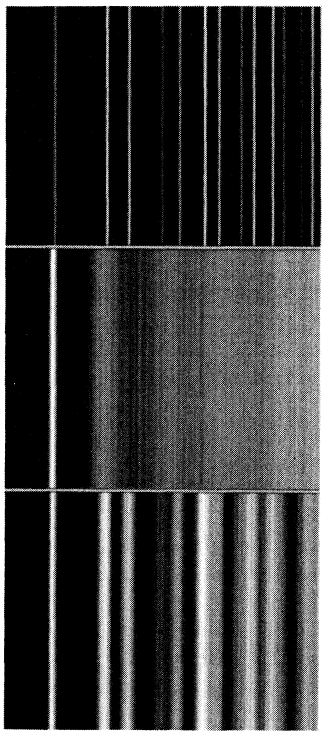

FIG. 4. Bar-code plots of the real-space distribution function $G(r)$ for an amorphous simulation (center plot) compared to those from the diamond structure (the diamond temperatures are $kT=0.01$ in the top plot and $kT=0.06$ in the bottom plot). The distance scale is linear, and increases from left to right.

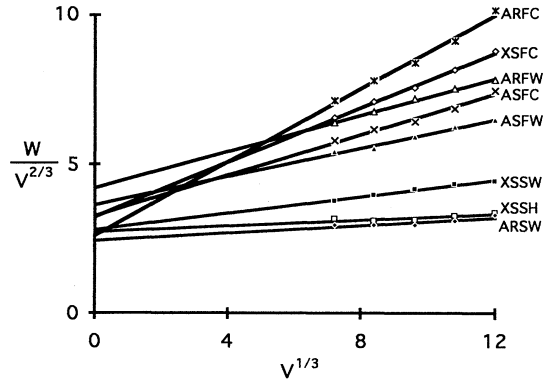

FIG. 5. The variation of the reduced work of the indentation, $W_{\text{total}}/V^{2/3}$ as a function of $V^{1/3}$, proportional to the indentation depth. The intercept gives an estimate of the combined elastic and surface energies while the slope is the plastic yield strength. The energy and length scales are given in Stillinger-Weber units (50 kcal/mole and 0.21 nm). The curves are identified by four sets of initials: [A = amorphous vs X = crystalline]; [R = rough vs S = smooth]; [F = fast vs S = slow]; and [C = cold vs W = warm vs H = hot: $kT=0.01$, 0.03, and 0.06, respectively].

accurate to 1%.

The indentor speed was kept constant (either 1.0 or 0.1 in Stillinger-Weber units) in our simulations. A speed of unity corresponds to 2.7 km/s, about one third the longitudinal sound speed. The amorphous material and the crystalline phase have similar strengths (138 and 179 kb at this high rate and at the lowest temperature, $kT=0.01$). Lower yield strengths, of order 30 kb, result near the melting temperature and at the slower velocity.

For the indented amorphous solid, neither diffraction analyses nor the angle-average pair density functions $G(r)$ shows any signs of crystallization. On the other hand, indentations of the *crystalline* phase did show, near melting and close to the indentor surface, a tendency to transform to the amorphous phase. Topological defects in solid silicon can be characterized most easily in terms of *ring statistics*. In the deformed crystal, near the indentor, relatively energetic rings of five and seven silicon atoms replace many of the unstrained six- and eight-member rings that characterize the perfect crystal. Correcting for surface effects, we find that approximately two thirds of the atoms near the indentor belong to a five- or seven-member ring. On that basis, we describe this noncrystalline region as two thirds converted to the true amorphous structure in which *every* atom belongs to a five- or seven-member ring.[11] On the other hand, the deformed region still retains a memory of the original crystal structure, as can be inferred from the third peak of the correlation function $G(r)$. The deformed region of the crystal, viewed instead as an amorphous solid, would be well on its way to crystallization if allowed to do so.[11]

The computed diffraction patterns of Fig. 3 and the corresponding distribution functions support this picture of partial transformation to the amorphous phase. We were able to divide the crystal data sets into $6\times6\times6=216$ separate cubic regions, computing diffraction patterns and pair distribution functions for each of them. In the vicinity of the indentor faces, and at the higher temperature $kT=0.06$, the diamond phase transforms to an amorphous structure characterized by diffuse diffraction rings. This transformation supports the interpretation[6] of Clark *et al.* of their transmission electron micrograph.

Just after our work was carried out, Minowa and Sumino[12] described surface-scratching experiments on crystalline room-temperature silicon which transformed the crystal to a crack-free stress-induced amorphous phase without heavy plastic deformation. Compelling evidence for their conclusion was their experimental diffraction pattern that clearly shows the halo rings characterizing amorphous material.

We were able to rule out localized transformations far from the indentor. Such deformation surfaces might be expected based on plastic slip-line solutions which predict the large-scale motion of "chunks" of solid within the indentation workpiece. Our numerical evidence indicates that plastic deformation occurs primarily in the three surface bulges near the indentor and in the region within three atomic diameters of the indentor. We have used free lateral and top boundaries in our simulations so as not to inhibit the formation of lattice defects.

Our nanometer-sized indentation simulations support the suggestion[6] that amorphous silicon *is* formed *under* the indentor. We find *no evidence* for the transformation, suggested by Pharr, Oliver, and Harding, to the β-Sn structure under warm indentation. Because the β phase is a relatively good conductor and the Stillinger-Weber potential takes no explicit account of electrons, our failure to generate a β phase is not surprising.

We find that the nanoyield strength of silicon lies between 25 and 250 kbars. This strength depends upon the structure, rate of deformation, and temperature of the sample.

With present-day massively parallel computers, it is feasible to extend these simulations to considerably larger specimens. For million-atom specimens the corresponding run times will be of the order of one month. We hope to report on such simulations in the future, as well as on hybrid schemes combining these atomistic simulations with conventional Lagrangian and smooth-particle-hydrodynamic continuum simulations.

We very much appreciate the advice of Brad Holian (LANL), M. Allison, D. Boercker, C. Grant, and N. Winter (LLNL). Work at the Lawrence Livermore National Laboratory was supported by UC-DOE Contract No. W-7405-Eng-48.

[1]W. G. Hoover, A. J. De Groot, and C. G. Hoover, Comput. Phys. **6**, 155 (1992).
[2]W. G. Hoover *et al.*, Phys. Rev. A **42**, 5844 (1990).
[3]F. H. Stillinger and T. A. Weber, Phys. Rev. B **31**, 5262 (1985).
[4]Ron Scattergood (private communication).
[5]G. M. Pharr, W. C. Oliver, and S. Harding, J. Mater. Res. **6**, 1129 (1991).
[6]D. R. Clarke *et al.*, Phys. Rev. Lett. **60**, 2156 (1988).
[7]B. L. Holian *et al.*, Phys. Rev. A **41**, 4552 (1990); W. G. Hoover, *Computational Statistical Mechanics* (Elsevier, Amsterdam, 1991).
[8]P. C. Weakliem and E. A. Carter, J. Chem. Phys. **96**, 3240 (1992).
[9]F. Wooten and D. Weaire, Solid State Phys. **40**, 1 (1987); F. Wooten, K. Winer, and D. Weaire, Phys. Rev. Lett. **54**, 1392 (1985).
[10]J. M. Holender and G. J. Morgan, J. Phys. C **3**, 7241 (1991).
[11]F. Wooten *et al.*, J. Non-Cryst. Solids **75**, 45 (1985).
[12]K. Minowa and K. Sumino, Phys. Rev. Lett. **69**, 320 (1992).

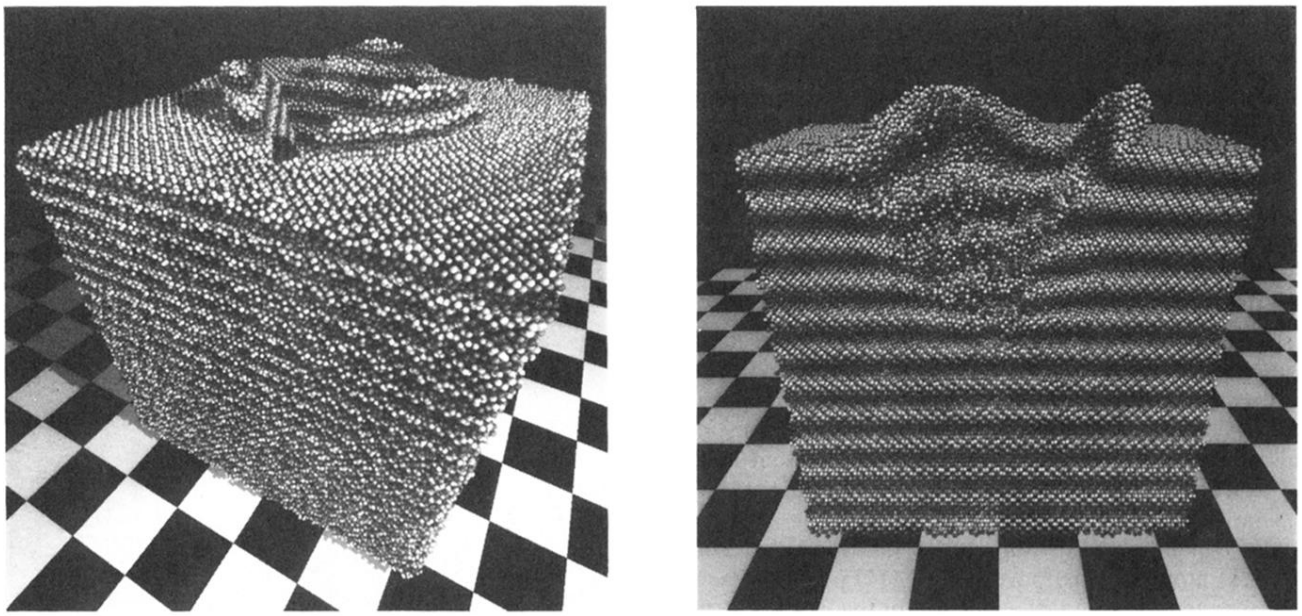

FIG. 1. The simulated indentation of crystalline Stillinger-Weber silicon. The left-hand view shows 373 248 silicon atoms, indented at a speed of 0.5 (about one sixth the speed of sound) and at a temperature $kT=0.03$, about half the melting temperature. The right-hand cutaway view of the same simulation reveals the plastic deformation in the vicinity of the indentation. The shading of the (left/right) figure is based on the (final/initial) vertical coordinates of the atoms.

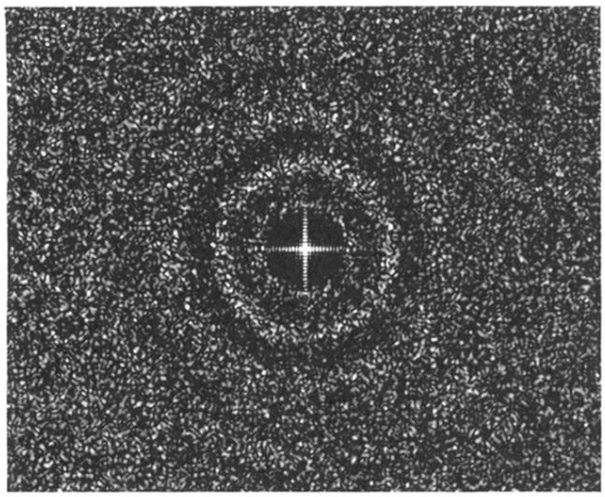

FIG. 2. The computational diffraction pattern for the Wooten-Weaire amorphous silicon structure used in our indentation simulations.

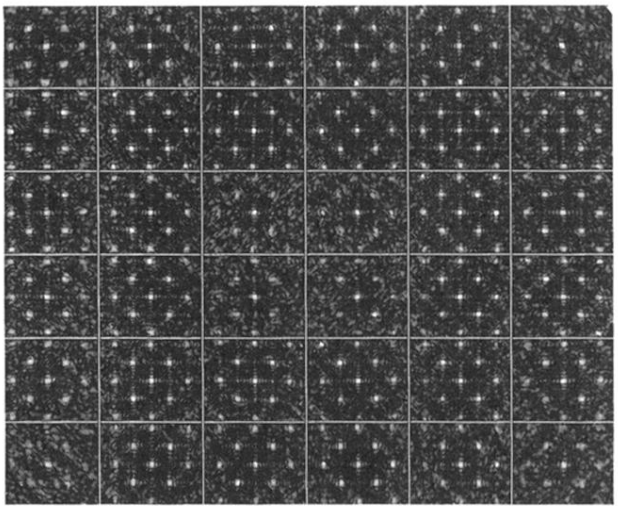

FIG. 3. 36 diffraction patterns from cubes just above the midplane of a 32 768-atom-indented silicon crystal with $kT = 0.06$, just below the melting point. The speed of the smooth indentor was 0.1.

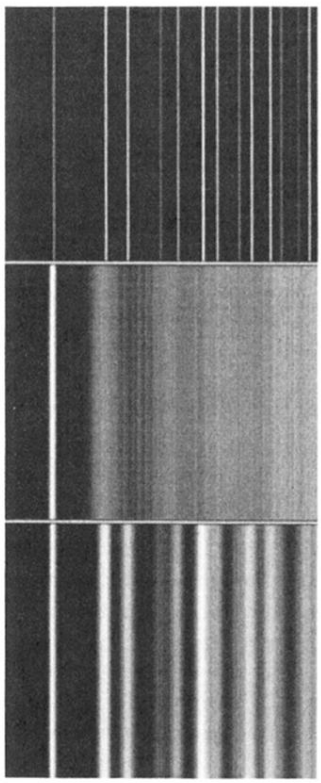

FIG. 4. Bar-code plots of the real-space distribution function $G(r)$ for an amorphous simulation (center plot) compared to those from the diamond structure (the diamond temperatures are $kT=0.01$ in the top plot and $kT=0.06$ in the bottom plot). The distance scale is linear, and increases from left to right.